

Accepted for publication in the June 2000 issue of the Publications  
of the Astronomical Society of the Pacific

## Volume–Phase Holographic Gratings and the Efficiency of Three Simple VPH Gratings

Samuel C. Barden

*National Optical Astronomy Observatories<sup>1</sup>, Tucson, AZ 85719*

*barden@noao.edu*

James A. Arns

*Kaiser Optical Systems, Inc., Ann Arbor, MI 48106*

*arns@kosi.com*

Willis S. Colburn<sup>2</sup>

*Ann Arbor, MI*

*wcolburn@mediaone.net*

and

Joel B. Williams

*National Optical Astronomy Observatories<sup>1</sup>, Tucson, AZ 85719*

*joelw@azstarnet.com*

### ABSTRACT

Volume–phase holographic (VPH) gratings show great potential as an alternative dispersing element to the classical surface–relief (SR) gratings presently used in most astronomical spectrographs. We present an introduction to this technology and give the results of an evaluation of three different VPH gratings: a  $300 \text{ l mm}^{-1}$  grating optimized at 1064 nm; a  $1200 \text{ l mm}^{-1}$  grating optimized at 532 nm; and a  $2400 \text{ l mm}^{-1}$  grating optimized for operation at 532 nm.

*Subject headings:* instrumentation: spectrographs

---

<sup>1</sup>Operated by the Association of Universities for Research in Astronomy, Inc. (AURA) under cooperative agreement with the National Science Foundation.

<sup>2</sup>Formerly of Kaiser Optical Systems, Inc.

## 1. INTRODUCTION

Holographic technology has been around now for several decades and has led to many innovative applications. Holographic surface-relief (SR) gratings have revolutionized ultra-violet astronomy through the fabrication of curved gratings with built-in aberration correction (Wolf 1976). Diffraction gratings based upon volume holograms rather than SR holograms have also been developed over the past twenty to thirty years and show great potential performance gains over their SR counterparts. However, the direct application of this technology for spectroscopic applications has only been made within the past decade with an emphasis in the area of Raman spectroscopy where these devices have been revolutionary. This technology, on the other hand, has gone relatively unnoticed by the astronomical community until only recently.

Barden, Arns, and Colburn (1998) first presented the performance and potential of volume-phase holographic (VPH) gratings for astronomical spectrographs through the analysis of a  $613 \text{ l mm}^{-1}$  VPH grating. The result of that work has spawned the development of several spectrographs utilizing VPH gratings at observatories around the world. To further understand the benefits and limitations of this grating technology, the authors obtained a grant from the National Science Foundation (NSF) to fabricate a total of eight VPH gratings for evaluation.

In this paper, we give an overview of the physics of VPH gratings and present the measured efficiency performance of three of the eight NSF gratings. The  $300$ ,  $1200$ , and  $2400 \text{ l mm}^{-1}$  gratings presented here represent gratings comparable in dispersion to most typical, first order, SR gratings. Followup papers will cover the performance of higher dispersion, first order VPH gratings; the performance of a reflective VPH grating; a dual frequency VPH grating; and the results of an attempt to fabricate a high order VPH grating. We will also present analysis of the wave-front and scattered light performance for the NSF gratings in a future paper.

As pointed out by Barden, Arns, and Colburn (1998), volume-phase holographic gratings provide many possible gains in performance capability over the typical astronomical gratings that are currently in use. Amongst the benefits are the following:

- VPH gratings can have potentially higher peak diffraction efficiency approaching 100% in many cases.
- Polarization effects in most VPH gratings are not as severe as in SR gratings.
- VPH gratings lack many of the grating anomalies apparent in ruled SR gratings.
- Ghosting and scattered light from a VPH grating is significantly reduced compared to ruled SR gratings.
- Some VPH gratings can be tuned to shift the diffraction efficiency peak to a desired wavelength.

- Some VPH gratings can also be tuned to direct the diffracted energy into higher orders of diffraction resulting in a versatility not possible with classical gratings.
- VPH gratings can be generated with higher line densities (up to  $6000 \text{ l mm}^{-1}$ ) than can SR gratings.
- These high line density gratings can be used in transmission with VPH grating technology unlike transmissive SR gratings that are generally restricted to line densities of less than  $1200 \text{ l mm}^{-1}$ ).
- Holographic technology is capable of producing very large VPH grating structures, up to and larger than 800 mm in diameter.
- A VPH grating can be cleaned due to the encapsulated nature of the grating itself.
- The encapsulated nature of a VPH grating allows the application of high performance, anti-reflection coatings on the surfaces of the element.
- VPH gratings are considerably easier to customize since each grating is likely to be an original rather than a replica, though replication processes do exist for VPH grating technology.
- Complex grating structures can be assembled into a VPH grating that are impossible to do with SR gratings.
- Transmissive VPH gratings can be designed to always work in the Littrow configuration resulting in a simplification of the camera objective optics on a VPH grating spectrograph.

The negative aspects of VPH gratings are:

- The wavelength and angular bandwidths for a VPH grating get very narrow for high line density transmission gratings and for reflection VPH gratings.
- The process for generating high order ( $m > 10$ ) VPH gratings is poorly understood at present making such gratings difficult or impossible to fabricate.
- A spectrograph must have a camera-to-collimator angle that conforms to the VPH grating parameters.

## 2. VPH GRATING PHYSICS

Rather than diffracting light by means of periodic surface structure as in either a ruled or holographically generated SR grating, a VPH grating diffracts light by fringes of refractive index

variations within the volume of the grating. Light is diffracted at angles according to the classical grating equation

$$m\nu\lambda = \sin(\alpha) + \sin(\beta) \quad (1)$$

in which  $m$  is the order of diffraction,  $\nu$  is the frequency of the intersection of the grating fringes with the grating surface,  $\lambda$  is the wavelength of light,  $\alpha$  is the angle of incidence from the grating normal in air, and  $\beta$  is the angle of diffraction measured to the grating normal in air. The diffracted energy distribution for a VPH grating, however, is governed by Bragg effects in a manner similar to the diffraction of X-rays by crystalline structures. The Bragg condition is given by

$$m\nu_g\lambda = 2n_g \sin(\alpha_g) \quad (2)$$

where  $\nu_g$  is the fringe frequency within the grating volume,  $n_g$  is the average refractive index of the grating medium, and  $\alpha_g$  is the angle of incidence inside the grating and measured with respect to the fringe plane. For the simplified case where the grating fringes are normal to the grating surface (unslanted), the Bragg condition can be represented by

$$m\nu\lambda = 2 \sin(\alpha) \quad (3)$$

where

$$n_g \sin(\alpha_g) = n \sin(\alpha) \quad (4)$$

with  $n$  assumed to be unity for air. The energy diffracted by the grating is usually a maximum when both wavelength and angle of the incident light satisfy the Bragg condition. Incident light that does not satisfy the Bragg condition is diffracted with less efficiency, and if the departure from the Bragg condition is substantial, most or all of the light passes through the grating undiffracted.

Four possible fringe orientations are displayed in Figure 1. The relationships between  $\alpha$ ,  $\beta$ ,  $\nu$ , and  $\Lambda = 1/\nu_g$  for the different structures can be seen in the figure. The first two configurations are transmission gratings, the third and fourth show reflection gratings. Note that the grating fringes do not intersect the grating surface in the third configuration. This results in zero dispersion of the light. When the fringe structure is normal to the grating surface, as in the first configuration, the grating will have zero anamorphic magnification at the Bragg wavelength corresponding to a Littrow configuration. Slanted or tilted fringes, as in the second and fourth configurations, introduce anamorphic magnification for both transmission and reflection gratings. The three gratings discussed in this paper are all of the type shown in case A of Figure 1.

The depth ( $d$ ) and index modulation contrast ( $\Delta n_g$ ) of the grating structure control the efficiency at which the light is diffracted when the Bragg condition is satisfied. Either rigorous coupled wave analysis (RCWA) (Moharam and Gaylord 1981; Gaylord and Moharam 1985) or modal analysis (Burckhardt 1966; Magnusson and Gaylord 1978) is generally required to theoretically model the diffraction efficiency of a VPH grating. However, Kogelnik (1969) developed a two-wave, first-order, coupled wave analysis that can be used to estimate the first order efficiency of a VPH grating. This approximation is valid when the following equation is satisfied

$$Q = \frac{2 \cdot \pi \cdot \lambda \cdot d}{n_g \cdot \Lambda^2} > 10. \quad (5)$$

For a transmission VPH grating with fringe structure normal to the grating surface, the diffraction efficiency for the two planes of polarization can be estimated by

$$\eta_s = \sin^2 \left[ \frac{\pi \cdot \Delta n_g \cdot d}{\lambda \cos(\alpha_g)} \right] \quad (6)$$

and

$$\eta_p = \eta_s \cos(\alpha_g + \beta_g) \quad (7)$$

in which  $\alpha_g$  and  $\beta_g$  are the angles of incidence and diffraction within the grating volume. The efficiency for the  $p$  plane of polarization does not differ significantly from the  $s$  plane as long as the sum of  $\alpha_g$  and  $\beta_g$  is not close to  $90^\circ$ . The grating becomes a perfect polarization beam splitter when the sum of those angles does equal  $90^\circ$  in which case only one of the polarization planes is diffracted and the other is passed straight through.

Peak diffraction efficiency, in the Kogelnik approximation, is achieved when the angle of incidence and the wavelength satisfy the Bragg condition, equation 2, and when the following relationship between wavelength, index modulation, and grating depth is nearly satisfied

$$\Delta n_g \cdot d \approx \frac{\lambda}{2}. \quad (8)$$

This relationship provides a good starting point in the design of most VPH gratings when the Bragg angle is relatively small. We note that as equation 6 indicates, the diffraction efficiency for transmissive VPH gratings is periodic as a function of the index modulation and depth. If either value is under or over the optimal value, a decrease in the diffraction efficiency will result.

Light that nearly satisfies the Bragg condition can also be diffracted with good efficiency depending on the grating parameters. For transmission gratings, as the angle of incidence is changed, the diffraction efficiency for a given wavelength is approximated by

$$\Delta \alpha_{FWHM} \propto \frac{\Lambda}{d} \quad (9)$$

where  $\Lambda$  ( $= 1/\nu_g$ ) is the fringe spacing within the grating. Likewise, as the wavelength deviates from the Bragg wavelength for a fixed grating angle, the efficiency is approximated by

$$\frac{\Delta \lambda_{FWHM}}{\lambda} \propto \frac{\Lambda}{d} \cot(\alpha_g). \quad (10)$$

$\Delta \alpha_{FWHM}$  and  $\Delta \lambda_{FWHM}$  are called the angular Bragg envelope and spectral Bragg envelope, respectively (Kogelnik 1969). In essence, the fringe frequency and depth ( $d$ ) of the grating volume control the bandwidth of the grating. Since the fringe frequency defines the grating dispersion, control over the bandwidth is maintained by picking an appropriate grating depth. This must be balanced against the diffraction efficiency of the grating which relies on the depth as well. Large bandwidth gratings require large values for the fringe contrast,  $\Delta n_g$ , and small values for the depth,  $d$ . In practice,  $\Delta n_g$  is limited to a maximum value of about 0.1 for current state of the art materials. This restricts the minimum value of  $d$  (at a few microns) for achieving maximum efficiency and bandwidth performance.

### 3. VPH GRATING STRUCTURE

The VPH gratings fabricated at Kaiser Optical Systems, Inc. (KOSI) are made with dichromated gelatin (DCG), a material that has been used extensively in holographic materials for the past several decades. DCG has a proven record of producing high quality diffraction elements with high diffraction efficiency, high clarity, low scatter, low absorption, and long lifetime when it is properly treated in the fabrication process and adequately protected against degrading environmental conditions (Shankoff 1968; Chang and Leonard 1979; Hariharan 1996). Because DCG is hygroscopic and must be protected from humidity, it is typically encapsulated between two plates of glass. Properly sealed and handled, DCG holograms can have lifetimes of at least 20 years. The routine use of DCG in head-up display components in the military demonstrate that such elements can survive exposure to significant humidity and temperature extremes.

The measured transmittance of a uniformly exposed and processed, 15  $\mu\text{m}$  layer of DCG is displayed in Figure 2. It is evident that DCG may have a useful spectral window from 300 nm to 2.8  $\mu\text{m}$ . KOSI currently has experience in making VPH gratings for use at wavelengths between 350 nm and 1.5  $\mu\text{m}$ . We note that the purity of the DCG must be quite high in order to minimize absorption bands that might otherwise reside in the 1 to 3  $\mu\text{m}$  window.

A VPH grating is made by depositing a thin film of sensitized DCG onto a glass substrate. A holographic exposure system is used to record an interferometrically produced wave pattern of the desired fringe frequency and orientation within the gelatin layer. The grating is then processed in a bath of water that swells the gelatin layer. Rapid dehydration of the gelatin in a subsequent alcohol bath causes the gelatin to collapse with a periodic variation in gelatin density. The final density depends on the level of light that was exposed onto that particular region of gelatin. The resultant material density translates directly into a specific value for the refractive index, so the original fringe pattern of the holographic exposure is imprinted into the grating as a modulation of its refractive index. Once the desired grating parameters have been achieved, a glass cover is laminated onto the gelatin surface.

The glass substrate and cover may be made from any type of glass material. BK7 and fused silica are most commonly used. The outer surfaces of the glass plates may also be coated with appropriate anti-reflection coatings to minimize surface reflections and spurious signals. It is also possible to utilize prisms and/or lenses within the grating assembly.

DCG has an average refractive index of about 1.5 and can be processed to deliver index modulations ranging from 0.02 to about 0.10 in layers as thick as 4 to greater than 20  $\mu\text{m}$ . Line densities of 300 to 6000  $\text{l mm}^{-1}$  can be recorded in the material. In general, the index modulation produced in DCG is assumed to be sinusoidal and can be represented by

$$n_g(x, z) = n_g + \Delta n_g \cos[(2\pi/\Lambda)(x \sin(\gamma) + z \cos(\gamma))] \quad (11)$$

where  $\gamma$  is the slant angle for the fringes (see Figure 1). In most cases, this approximation is valid, but as will be discussed below, the fringe structure may not be purely sinusoidal.

## 4. NSF STUDY

KOSI has been fabricating VPH gratings for utilization in Raman spectroscopy for several years (Tedesco, Owen, Pallister, and Morris 1993; Owen, Battey, Pelletier, and Slater 1995; Arns 1995). To evaluate the potential of VPH gratings for astronomical spectroscopy, Barden, Arns, and Colburn (1998) evaluated a  $613 \text{ l mm}^{-1}$  grating designed for optimal efficiency at 700 nm of 70 to 80% with a bandwidth adequate to cover the spectral range of 500 to 900 nm. At a grating angle of 11 to 12°, the grating delivers greater than 55% efficiency for unpolarized light across the 500 to 900 nm band with peak efficiency of nearly 80% between 600 and 700 nm. This efficiency is 5 to 10% better than a comparable Bausch and Lomb SR grating in use at Kitt Peak National Observatory.

One of the most surprising aspects of the grating is its tunability with grating angle. The efficiency envelope, or blaze profile, can be shifted in wavelength by simply tilting the grating with respect to the incident beam in accordance with the Bragg condition defined in equation 2. At a tilt angle of 8°, the grating efficiency is 75% between 400 and 500 nm and remains above 50% to a wavelength near 800 nm. At a tilt angle of 25°, the grating diffracts over 65% of the light at 700 nm into the second order of diffraction. At 400 nm, efficient second and third order diffraction can be achieved by tilting the grating to angles of 14 and 21° respectively.

Given these results, the authors obtained funding from the National Science Foundation to further explore the capabilities of this intriguing technology. Eight VPH gratings were fabricated at KOSI for evaluation. Table 1 lists the parameters for all eight gratings.

Each grating was measured for its efficiency as a function of wavelength and grating tilt in unpolarized light. Wavefront performance was evaluated for most of the gratings. Scattered light was also estimated for a few of the gratings. In addition, a simple on-sky test was performed with a fiber optic feed on the 2.1-meter telescope at Kitt Peak National Observatory for some of the gratings.

The efficiency performance of gratings 1, 2, and 3 are presented here. Future papers will address the characteristics of the remaining gratings listed in Table 1. Scattered light and wavefront evaluation will also be given in a future paper that will summarize the performance of all the gratings that were so evaluated.

## 5. GRATING EFFICIENCY

### 5.1. Efficiency Measurements

Most of the efficiency measurements in unpolarized light were obtained at the National Optical Astronomy Observatories (NOAO) in the following manner. A Perkin Elmer, Lambda9 spectrophotometer was used to scan the  $m = 0$  diffraction order with the grating illuminated at  $\alpha =$

0°. Relative efficiencies were made on an optical bench layout at a variety of wavelengths, grating angles, and diffraction orders all with respect to the  $m = 0$ ,  $\alpha = 0$  efficiency for each wavelength. Absolute total efficiencies were derived by scaling the relative measurements with the values measured by the Perkin Elmer spectrophotometer. We note that the substrate and surface reflection losses are included in the measured efficiencies. If the grating has an anti-reflection (AR) coating that was applied for minimal surface reflection loss at the design grating angle, then that coating may reduce the overall efficiency of the grating as it is used at angles other than the design angle. We do not distinguish this effect for any of the gratings in the data presented.

In the setup to measure the relative efficiencies, a current-stabilized quartz lamp fed into a monochromator via a fiber optic bundle. A 50  $\mu\text{m}$  fiber optic, located at the exit slit of the monochromator, transferred the monochromatic light to the focal point of a collimating lens. That lens produced a 40 mm diameter beam that illuminated the grating. The grating was mounted on an adjustable stage for tip-tilt alignment and rotation in angle ( $\alpha$ ). The camera lens and CCD detector were positioned on a rail that could pivot in angle ( $\theta$ ) about the grating axis. For the efficiency measurements, the CCD was moved forward of focus in order to spread the light over a large number of pixels to increase the detected signal-to-noise of the measurement.

Each data set contains repeated measurements for the  $\alpha = 0$  and  $\theta = 0$  position. These serve as the data points for scaling the relative measurements into absolute measurements. For a given wavelength, the data were taken with the camera at a fixed angle  $\theta$ , corresponding to the diffraction order under evaluation, and the grating rotated in  $\alpha$  over a range of angles (typically from  $-5$  to  $45^\circ$ ) in increments of  $1^\circ$ . Full scans in  $\alpha$  were obtained for the wavelengths of 400, 600, 800, and 1000 nm in order to provide some data for comparison with theoretical models. Subsets of a full scan were obtained for 375, 450, 500, 550, 650, 700, 750, 850, 900, 950, and 1050 nm in which  $\alpha$  was only rotated over the angles that provided more than about 10% diffraction efficiency for the diffraction order under investigation.

The data, collected with an SBIG ST-6 UV enhanced camera, were transferred into IRAF<sup>3</sup> and reduced by performing aperture photometry on the image. The signal for each image was divided by the average value of the contemporaneous  $\alpha = 0$  and  $\theta = 0$  measurements. Absolute efficiencies were derived by scaling each value by the corresponding value measured with the Perkin Elmer, Lambda9 spectrophotometer.

The spectral bandwidths are taken from the “blaze” profile at the full width, half maximum values. Angular bandwidths were measured at KOSI (Arns, Colburn, and Barden 1999) at a variety of laser wavelengths.

---

<sup>3</sup>IRAF is distributed by the National Optical Astronomy Observatories.

## 5.2. Theoretical Models

Theoretical predictions for the diffraction efficiency of each grating was performed with a program called GSOLVER©4.0<sup>4</sup>. The program approximates grating structures in a piecewise manner and evaluates the diffraction efficiency with RCWA and modal theory. The modeling of sinusoidal, VPH gratings with the fringe structure normal to the grating surface is straightforward and matches the output of other RCWA programs. The piecewise approach also allows the modeling of VPH gratings with non-sinusoidal profiles and of gratings with tilted fringes. GSOLVER can also model low order, classical SR gratings either in transmission or with a reflective coating.

### 5.3. 300 l mm<sup>-1</sup> VPH Grating Efficiency

Grating 1 in Table 1 was fabricated for optimal performance at 1064 nm with a FWHM spectral bandwidth goal of 500 nm. The 72 by 72 mm grating is sandwiched between two 3-mm, uncoated, BK7 substrates with an overall dimension of 77 by 93 mm. A clear area, 18 by 77 mm in size, is located at one edge of the grating for comparison of the substrate properties to that of the grating. The spectral dispersion is along the short axis of the grating dimensions. The grating, designated HG-T-1064-9 (HG stands for holographic grating, T for transmissive, 1064 for the design wavelength of 1064 nm, and 9 for the diffraction angle of the design wavelength in the first order of diffraction), had a lower line frequency (300 l mm<sup>-1</sup>) than had been produced before at KOSI. As such, its fabrication represented somewhat of a challenge. The design parameters were a grating depth ( $d$ ) of 20  $\mu\text{m}$ , an index modulation ( $\Delta n_g$ ) of 0.020, fringe structure normal to the grating surface, and an operational Bragg angle of 9.18°. The predicted performance of this grating is given in Figure 3. That figure also shows the RCWA predicted performance of comparable SR reflection and transmission gratings.

Figures 4 and 5 display the tunable nature of this grating at 400 and 800 nm as a function of grating angle ( $\alpha$ ) and diffraction order ( $m$ ). Comparison of this data with that predicted by the RCWA model showed a significant discrepancy between the measured efficiency and that predicted, especially for the higher orders of diffraction. Better matches could not be found by merely changing the values used in the model for the grating thickness and the modulation intensity (Figure 6). We then explored models in which the fringe structure is no longer purely a sinusoid in shape (Case and Alferness 1976; Blair and Solymar 1990). Trial profiles containing higher Fourier terms within the index modulation showed that the modulation shape with a saturation at the higher levels of refractive index gave a better fit to the measured data. Regions with high, or more positive, values of refractive index are those regions that correspond to exposure to the bright fringes of the laser interference pattern. A model was generated based upon the assumption that saturation of the achievable index value flattens out the index profile.

---

<sup>4</sup>GSOLVER is a product of Grating Solver Development Company, P.O. Box 353, Allen, Texas 75013.

For unslanted fringes (configuration A of Figure 1), the holographic exposure system generates an interference pattern with the following energy profile

$$E(x) = E_{ave} + E_{amp} \cdot \sin(x), \quad (12)$$

where  $E_{ave}$  is the average exposure level and  $E_{amp}$  is the amplitude of the exposing fringe pattern. The index modulation in the grating is assumed to have a form defined by the following equation

$$\Delta n_g = \Delta n_{g,max} \left( 1 - e^{-aE(x)} \right), \quad (13)$$

in which  $a$  is a constant and  $\Delta n_{g,max}$  is the saturation value for the index modulation,  $\Delta n_g$ .

Figure 7 shows the modulation profile for a non-sinusoidal model in which  $E_{ave}$  is set to 550 mJ/cm<sup>2</sup>,  $E_{amp}$  equals 550 mJ/cm<sup>2</sup>,  $a$  is 0.0035, and  $\Delta n_{g,max}$  has a value of 0.0384. This profile and a grating depth of 22  $\mu$ m were used in GSOLVER to derive better fits to the measured data as displayed in Figure 8. It is this non-sinusoidal behavior of the modulation that may allow higher-order gratings to be fabricated with this technology.

The diffraction efficiency envelope in unpolarized light for the 300 l mm<sup>-1</sup> VPH grating at a variety of grating angles are displayed in Figures 9, 10, and 11. At 6° (Figure 9), the peak diffraction efficiency in first order approaches 80% at a wavelength of 750 nm while second order diffraction peaks near 400 nm with an efficiency of 60%. At a grating angle of 12° (Figure 11), the grating delivers nearly 60% efficiency at 700 nm and 500 nm in the second and third orders of diffraction, respectively. Fourth order diffraction at 350 nm is achieved with 45% efficiency.

This grating demonstrates a significant range of versatility that can not be achieved with a single, SR grating. Blazed SR gratings can not be tuned in this manner. Although a spectrograph utilizing a SR grating can be configured in almost any configuration without significantly compromising the “fixed” diffraction efficiency of the SR grating, such a spectrograph would require multiple gratings in order to cover the versatility of a tunable VPH grating spectrograph.

The 300 l mm<sup>-1</sup> VPH grating did not quite meet the expected efficiency performance at the design wavelength of 1064 nm, but yields excellent efficiencies at bluer wavelengths and provides significant versatility in spectral coverage and dispersing power through its tunable nature. The spectral bandwidth specification of 500 nm is easily met by this grating in its nominal configuration.

#### 5.4. 1200 l mm<sup>-1</sup> VPH Grating Efficiency

HG-T-532-19, grating 2 in Table 1, was designed to have optimal performance at 532 nm with a FWHM spectral bandwidth goal of 200 nm when operated at 18.61°. The grating area is 72 by 72 mm with substrate dimensions of 76 by 108 mm. The BK7 substrates are each 3-mm thick with simple MgF<sub>2</sub> quarter-wave anti-reflection coatings. A blank region of 32 by 76 mm is located at one end of the assembly for efficiency comparisons. The spectral dispersion for this grating is along

the long dimension of the grating assembly. This grating was fabricated with a line frequency of  $1200 \text{ l mm}^{-1}$ , a grating depth of  $4 \mu\text{m}$ , and an index modulation of 0.065 with fringes normal to the grating surface. The theoretical performance is shown in Figure 12 along with the theoretical performance of comparable SR reflection and transmission gratings.

This grating is also tunable, as displayed in Figure 13 that shows efficiency measurements made at 400 nm. The measured efficiency of the  $1200 \text{ l mm}^{-1}$  VPH grating at its design Bragg angle of  $19^\circ$  is shown in Figure 14. Also displayed in that figure is the curve labeled the “superblaze”. The “superblaze” shows the peak diffraction efficiency of the grating as the grating is tuned in angle ( $\alpha$ ). The wiggles in the “superblaze” shown in the figure are an artifact due to the relatively coarse sampling in both angle ( $\alpha$ ) and wavelength.

Although the bandwidth of the VPH grating is narrower for a fixed grating angle than that provided by a comparable SR grating, the tunability of the VPH grating allows it to match, or exceed, the performance of the SR grating across the full operational range of both gratings as long as spectral coverage is not compromised by the bandwidth of the VPH grating when tuned to the desired wavelength. This is bound to be the case for relatively small format detectors where the detector, not the bandwidth of the VPH grating, limits the spectral coverage. For larger format detectors, the bandwidth issue must be considered in the tradeoff between implementation of either a VPH or classical SR grating.

In general, the  $1200 \text{ l mm}^{-1}$  VPH grating meets the efficiency of the theoretical predictions and achieves a peak efficiency of 87% at 500 nm. The spectral bandwidth for this grating is about 300 nm at the design wavelength exceeding the original specification of 200 nm. The angular bandwidth was measured to be  $15^\circ$  at 532 nm.

### 5.5. $2400 \text{ l mm}^{-1}$ VPH Grating Efficiency

The third grating, HG-T-532-40, in Table 1 is a  $2400 \text{ l mm}^{-1}$  grating designed for peak operation at 532 nm with a spectral bandwidth goal of 60 nm. This 72 by 72 mm grating is mounted between two 8 mm, BK7 substrates. The substrates, 76 by 102 mm, have a simple  $\text{MgF}_2$  anti-reflection coating applied to their outer surfaces. As in the other gratings, the grating itself is offset in the assembly in order to provide a blank region for evaluation of the substrate transmission efficiency. The spectral direction is parallel to the long axis of the grating assembly. The design parameters for this grating were a depth of  $4 \mu\text{m}$ , an index modulation of 0.072, fringe structure normal to the grating surface, and a Bragg angle of  $39.7^\circ$ . Figure 15 displays the theoretical efficiency for this grating assuming sinusoidal index modulations. The theoretical performance of a comparable SR grating is also shown in the figure. We note that it is effectively impossible to fabricate a working  $2400 \text{ l mm}^{-1}$  transmission SR grating due to the fact that the groove angles are so steep that internal reflections become a dominant source of efficiency loss. The deep grooves also complicate the replication process making it difficult to cleanly separate the replica from the

master.

Figure 16 shows the efficiency of HG–T–532–40 as a function of grating angle at 400 nm. Note the narrow angular bandwidth.

Figure 17 gives the “blaze” profile in unpolarized light for the 2400 l mm<sup>−1</sup> VPH grating when tuned to Bragg angles of 27, 33, 37, 40, and 46°. The “superblaze” is also overplotted in the figure. Wiggles in the “superblaze” arise from the 1° sampling interval for the grating angle ( $\alpha$ ) and from the 50 nm sampling in wavelength. We note that the AR coating for this grating was optimized for minimal reflective losses at the design grating angle of 40°. When this grating is tuned away from that angle, the surface reflection losses may become a fairly significant factor in the loss of efficiency, particularly at angles significantly different from 40°.

The peak efficiency of this grating reaches nearly 88% when the grating is tuned to operate at a Bragg wavelength of 440 nm. The spectral bandwidth for this grating (110 nm) exceeds the original goal of 60 nm by nearly a factor of two. The angular bandwidth was measured at 6.5° for the design wavelength of 532 nm.

## 5.6. On–Sky Performance

The viability of VPH gratings for astronomical spectroscopy is best demonstrated with real astronomical spectra obtained with VPH gratings. Barden, Arns, and Colburn (1998) presented the first known astronomical spectrum taken with the original 613 l mm<sup>−1</sup> test VPH grating. The first science conducted with a VPH grating was performed at the Anglo–Australian Observatory where they retrofitted a 400 l mm<sup>−1</sup> VPH grism into the LDSS++ instrument (Glazebrook et al. 1998, 2000). The redshifts of numerous objects in the Hubble Deep Field South as faint as R=24 were obtained (Glazebrook and Monbleau 2000).

To further verify the viability of VPH gratings, some on–sky testing was performed for the 300 (HG–T–1064–9) and 2400 l mm<sup>−1</sup> (HG–T–532–40) VPH gratings using a fiber optic feed on the 2.1–meter telescope at Kitt Peak National Observatory in late April of 1999. The fiber optic cable, 30 meters in length, subtended 2.5 arc–seconds on the sky and fed into a simple spectrograph, the QDS (quick and dirty spectrograph). The QDS consisted of three achromatic lenses, the test VPH grating, an order sorting filter, and a 2048 by 2048 CCD detector (T2KB). The detector was binned into a 512 by 512 format in order to better match the image formed by the spectrograph.

### 5.6.1. 300 l mm<sup>−1</sup> Grating

Three observations of the spectrophotometric flux standard star, Feige 34, were made with grating HG–T–1064–9 at three different grating angles (4, 6, and 7.6°). The overall system efficiency (including telescope, fiber optic, seeing, spectrograph, and detector efficiencies) or detected

quantum efficiency (DQE) measured with these observations was analyzed. At  $4^\circ$  the DQE was 2.2% at 400 nm, 5.1% at 450 nm, 6.7% at 500 nm, and 7.6% at 550 nm. When adjusted to a grating angle of  $6^\circ$ , the DQE was measured to be 5.9% at 650 nm, 8.0% at 700 nm, 7.6% at 750 nm, and 6.3% at 800 nm. The spectra obtained at the grating angle of  $7.6^\circ$  were compromised by the presence of the OH absorption bands in the fiber optic cable.

The seeing was not particularly good on that night, 29 April, 1999, with measured values of 2.6 arc-seconds for the  $4^\circ$  observations, and 2.2 arc-seconds for both the  $6^\circ$  and  $7.6^\circ$  data. This results in a loss of nearly 65% of the stellar photons on the circular fiber aperture alone. Additionally, the primary and secondary mirrors of the 2.1-meter telescope had not been aluminized for nearly five years and it is expected that scattering due to the poor coating further suppressed the signal in the core of the stellar image. The effect of seeing was particularly noticeable on the night of 1 May, 1999, during which the NSF multiplex grating (grating 6 in Table 1) was tested. Although not spectacular, the seeing on that night was considerably better than on the previous two nights, measured at 1.2 arc-seconds. As such, the fiber aperture should only lose about 25% of the light in the image profile and the total system DQE was measured to peak at a value of 29% (Barden, Williams, Arns, and Colburn 2000)! Consequently, we believe that the DQE for the HG-T-1064-9 grating was dominated by poor seeing effects and that the grating was performing as evaluated in the lab.

### 5.6.2. $2400\text{ l mm}^{-1}$ Grating

On the night of 30 April, 1999, the  $2400\text{ l mm}^{-1}$  VPH grating, HG-T-532-40, was used to observe the flux standard, HZ 44, in addition to observations of M57 and a bow shock in NGC 4258 with a grating angle of  $36^\circ$ . Clouds prevented any observations during the first portion of the night. After the skies cleared up, the seeing was measured to be about 2.2 arc-seconds. The total system DQE was determined by the HZ 44 observation to be 11% across the spectrum from 485 to 500 nm. Again, this efficiency was dominated by losses on the circular, fiber aperture due to the poor seeing.

## 6. Concluding Remarks

VPH grating technology has a lot to offer for use in astronomical applications. The diffraction efficiencies can be considerably higher than those obtained with classical SR gratings and with less dependence on the polarization state of the light being analyzed. The encapsulated nature of VPH gratings allow them to be better protected from environmental factors and allows the cleaning of the outer surfaces. The transmissive, Littrow configuration results in simplification of the camera optics where the emphasis of the camera can be dedicated to the field of view desired in the spectrograph rather than to the anamorphic magnification introduced by using gratings in

an off-Littrow configuration. The ability to make complex grating configurations provides unique advantages of VPH grating technology over SR gratings.

Caution must be made with respect to the spectrograph configuration that utilizes VPH gratings as the camera to collimator angle must match the Bragg angle of the grating. In addition, careful attention is required to ensure that the angular and wavelength bandwidths of the VPH grating are not exceeded. This is not a significant issue for the low line frequency gratings, but becomes more pronounced as the line density increases.

There are currently efforts underway to build VPH grating spectrographs at the following institutions or observatories with similar interest increasing at many other institutions: NOAO, the Anglo-Australian Observatory, the SOAR Observatory, and the University of Michigan for the Magellan Observatory. VPH grisms have been fabricated for use in the LDSS++ instrument at the Anglo-Australian Observatory and at the European Southern Observatory. Grating HG-T-1064-9 has also recently been loaned to Dr. Uwe Fink at the Lunar and Planetary Lab of the University of Arizona for implementation and replacement of a transmissive SR grating in a transmissive grating spectrograph that has an ideal configuration for this VPH grating. We also note that some of the remaining NSF gratings will become available for loan to the US astronomical community at the conclusion of the NSF study.

This work was funded under Cooperative Agreement AST-9613615 awarded by the National Science Foundation. The authors express their great appreciation to Ben Snavely, formerly at the NSF, for funding the grant through the Advanced Technologies and Instrumentation program of the NSF Astronomy division. The additional support provided by Richard Green and Sidney Wolff at NOAO were invaluable for this effort. Corporate support by John Ward, president of Kaiser Optical Systems, Inc., was also appreciated and necessary for this project to proceed. Sincere gratitude goes to Mark Benson for his dedication and efforts in constructing and evaluating the VPH gratings at KOSI. Thanks go to Skip Andree at NOAO for his support in setting up the QDS instrument for the on-sky testing of the gratings. We also thank Keith Taylor and Gordon Robertson of the Anglo-Australian Observatory for productive discussions that led to the term “superblaze”. Chris Clemens is acknowledged for his simplified insight into the Kogelnik approximations. S. Barden also thanks Tom Ingerson at Cerro Tololo Interamerican Observatory for his expression of interest which helped motivate the assembly of the successful NSF proposal. We thank Dan Schroeder for his comments on the manuscript which helped enhance its readability.

## REFERENCES

- Arns, J. A. 1995, Proc. SPIE, 2404, 174
- Arns, J. A., Colburn, W. S., and Barden, S. C. 1999, Proc. SPIE, 3779, 313
- Barden, S. C., Arns, J. A., and Colburn, W. S. 1998, Proc. SPIE, 3355, 866

- Barden, S. C., Williams, J. B., Arns, J. A., and Colburn, W. S. 2000, ASP Conf. Ser., 195, in press
- Blair, L. T. and Solymar, L. 1990, Optics Communications, 77, 365
- Burckhardt, C. B. 1966, J. Opt. Soc. Amer., 56, 1502
- Case, S. K. and Alferness, R. 1976, Applied Physics B, 10, 41
- Chang, B. J. and Leonard, C. D. 1979, Appl. Opt., 18, 2407
- Gaylord, T. K. and Moharam, M. G. 1985, Proc. IEEE, 73, 894
- Glazebrook K., Bland–Hawthorn J., Farrell T.J., Waller L. G., Barton J.R., Taylor K. 1998, AAO Newsletter 87
- Glazebrook K., Bland–Hawthorn J., Farrell T.J., Waller L. G., Barton J.R., Taylor K. 2000, in preparation
- Glazebrook K., Monbleau D.N. 2000, MNRAS, in preparation
- Hariharan, P. 1996, Optical Holography: Principles, Techniques, and Applications, Cambridge University Press, Second Edition, 107
- Kogelnik, H. 1969, The Bell System Technical Journal, 48, 2909
- Magnusson, R. and Gaylord, T. K. 1978, J. Opt. Soc. Amer., 68, 1777
- Moharam, M. G. and Gaylord, T. K. 1981, J. Opt. Soc. Amer., 71, 811
- Owen, H., Battey, D. E., Pelletier, M. J., and Slater, J. B. 1995, Proc. SPIE, 2406, 260
- Shankoff, T. A. 1968, Appl. Opt., 7, 2101
- Tedesco, J. M., Owen, H., Pallister, D. M., and Morris, M. D. 1993, Analytical Chemistry, 65, 441A
- Wolf, E. 1976, Progress in Optics, 14

Table 1. List of NSF grating parameters.

| Grating            | $\nu$<br>( $1 \text{ mm}^{-1}$ ) | $\lambda$<br>(nm) | $m$ | Bandwidth<br>(nm) | Comment                          |
|--------------------|----------------------------------|-------------------|-----|-------------------|----------------------------------|
| 1 (HG-T-1064-9)    | 300                              | 1064              | 1   | 500               | Transmission Grating             |
| 2 (HG-T-532-19)    | 1200                             | 532               | 1   | 200               | Transmission Grating             |
| 3 (HG-T-532-40)    | 2400                             | 532               | 1   | 60                | Transmission Grating             |
| 4 (HG-PTP-1064-3)  | 2400                             | 1064              | 1   | 50                | Trans. Grating, Prism Substrates |
| 5 (HG-PTP-532-4)   | 4800                             | 532               | 1   | 25                | Trans. Grating, Prism Substrates |
| 6 (HPG-656/486-23) | 1200/1620                        | 656/486           | 1   | 150               | Dual Frequency Trans. Grating    |
| 7 (HG-T6-532-26.7) | 300                              | 532               | 6   | 100               | High Order Trans. Grating        |
| 8 (HG-R-532-4/34)  | 1200                             | 532               | 1   | 200               | Reflection Grating               |

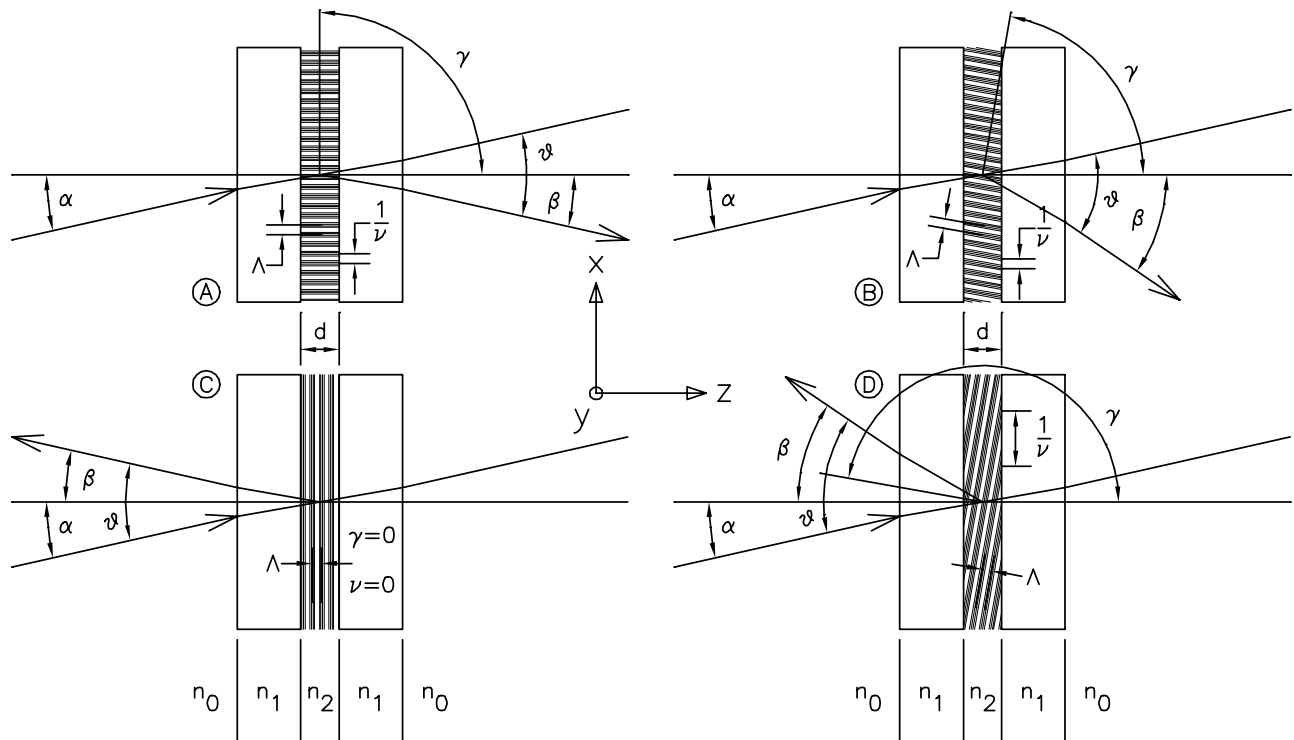


Fig. 1.— Four possible fringe structures for VPH gratings: A) Littrow transmission grating. B) Non-Littrow transmission grating. C) Non-dispersive reflection grating (notch filter). D) Dispersive reflection grating.

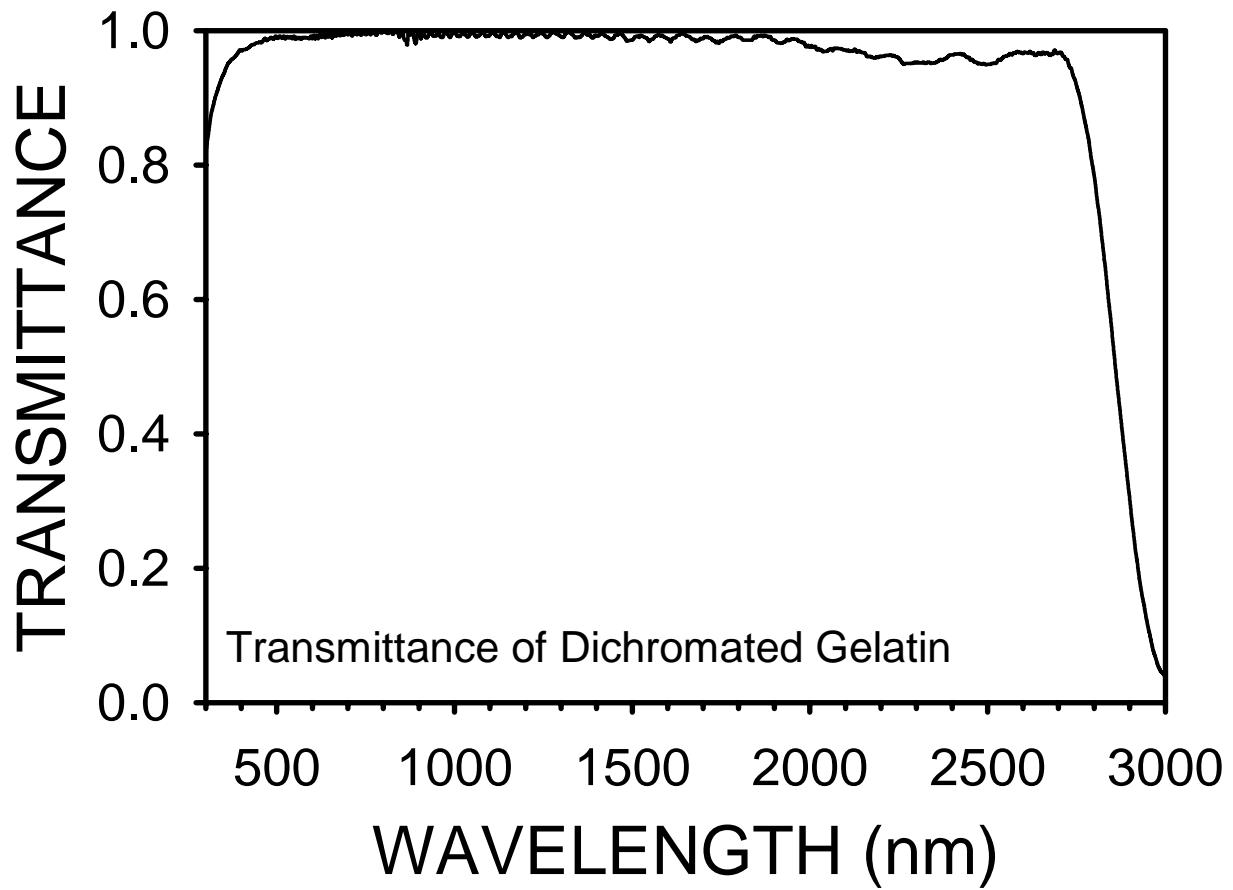


Fig. 2.— The transmittance of dichromated gelatin (DCG) uniformly exposed and processed with a  $15 \mu\text{m}$  depth. The transmittance of the BK7 substrate and surface reflection losses were ratioed out.

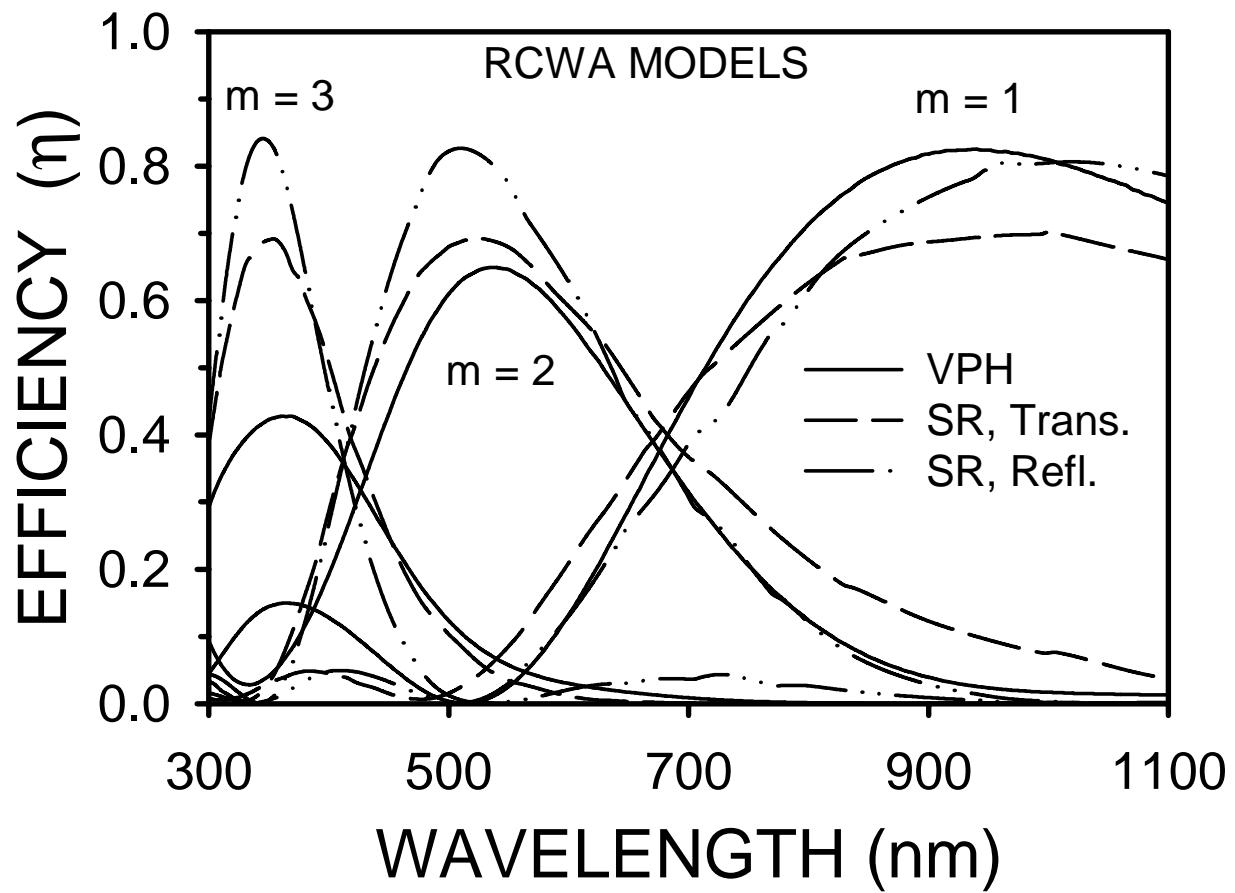


Fig. 3.— RCWA predicted efficiency for the  $300 \text{ l mm}^{-1}$  VPH grating (HG-T-1064-9) and comparable SR reflection and transmission gratings. A purely sinusoidal index modulation was assumed for the VPH grating. The first three orders of diffraction are shown.

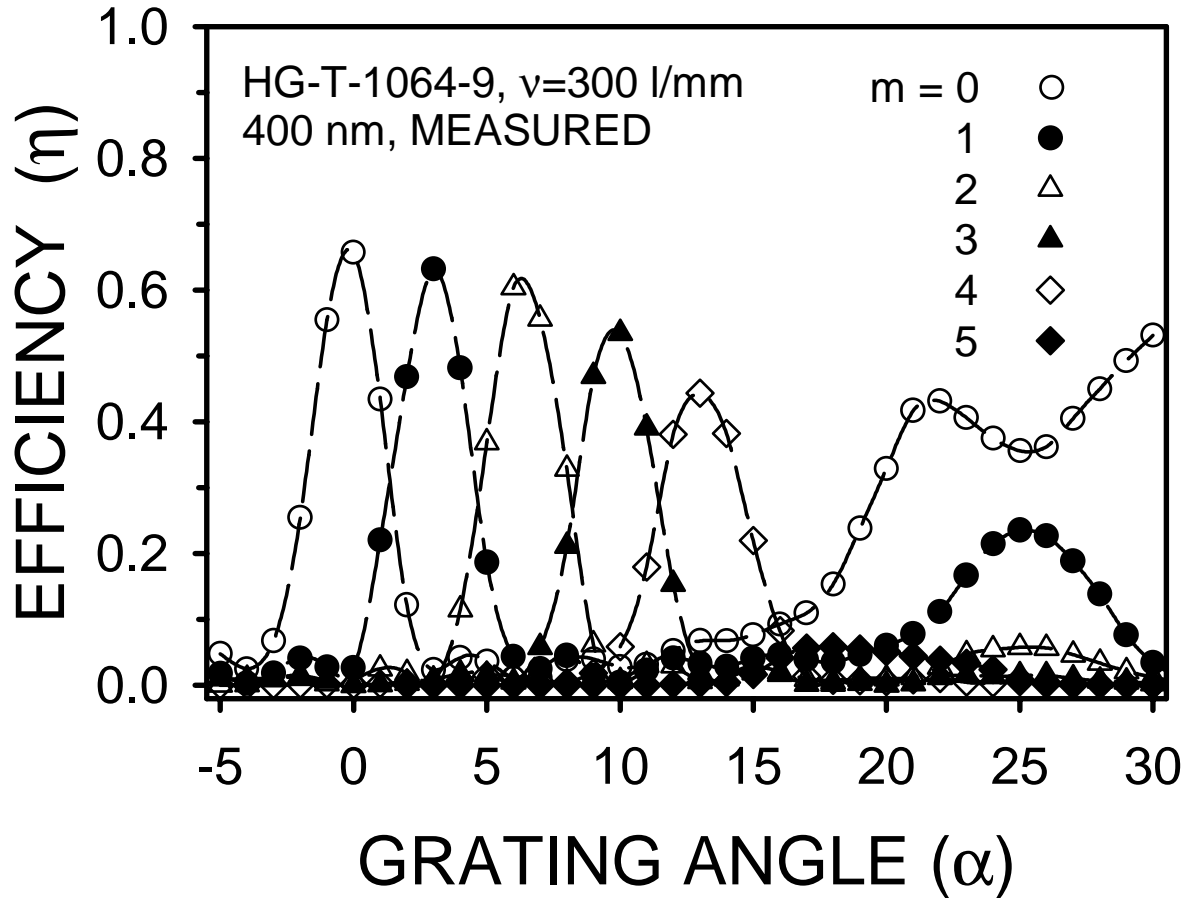


Fig. 4.— Measured absolute efficiency, inclusive of substrate material and surface reflection losses, in unpolarized light for the  $300 \text{ l mm}^{-1}$  VPH grating (HG-T-1064-9) at 400 nm as a function of diffraction order ( $m$ ) and grating angle ( $\alpha$ ). There is significant diffraction efficiency in the first four orders of diffraction. The fifth order shows very little efficiency (less than 10%).

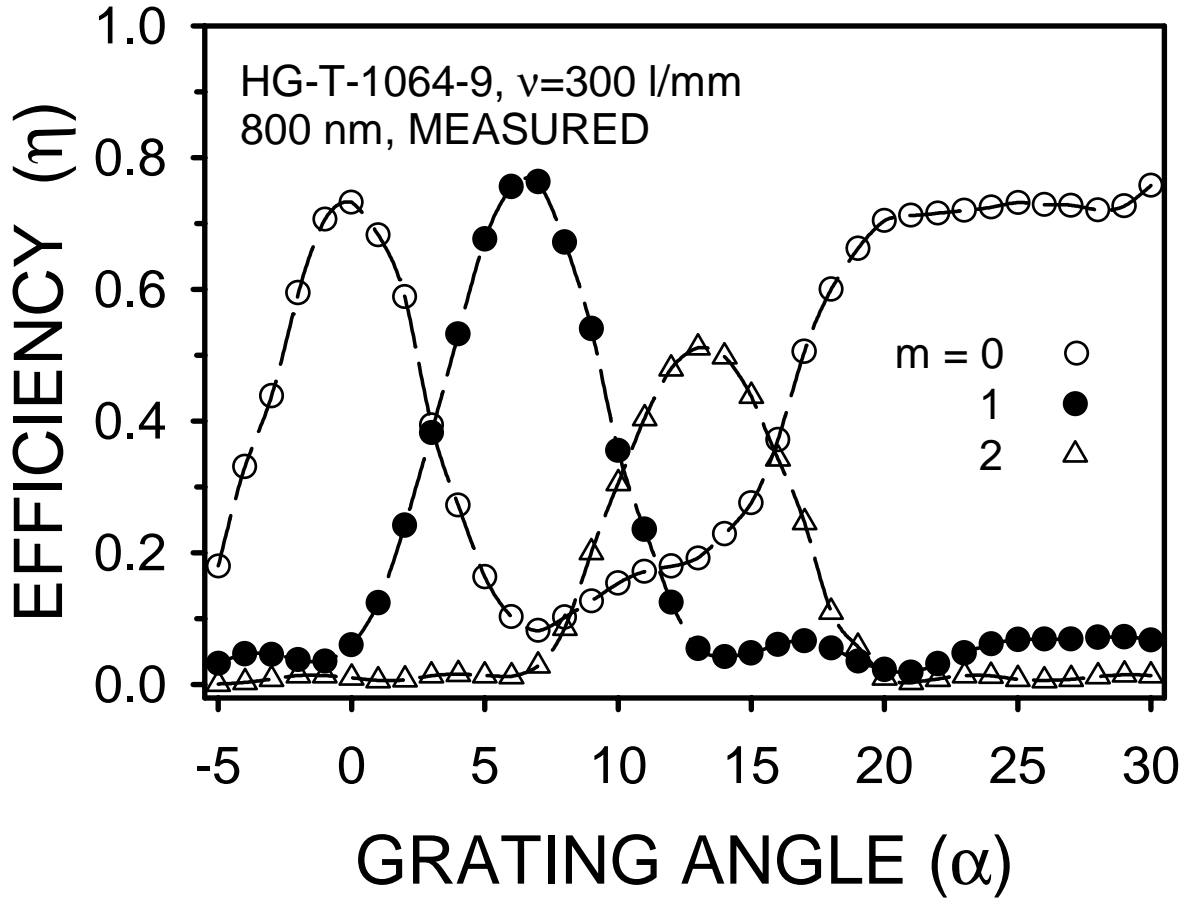


Fig. 5.— Measured absolute efficiency, inclusive of substrate material and surface reflection losses, in unpolarized light for the  $300 \text{ l mm}^{-1}$  VPH grating (HG-T-1064-9) at 800 nm as a function of diffraction order ( $m$ ) and grating angle ( $\alpha$ ). There is considerable efficiency in the second order of diffraction that can not be accounted for by a purely sinusoidal index modulation.

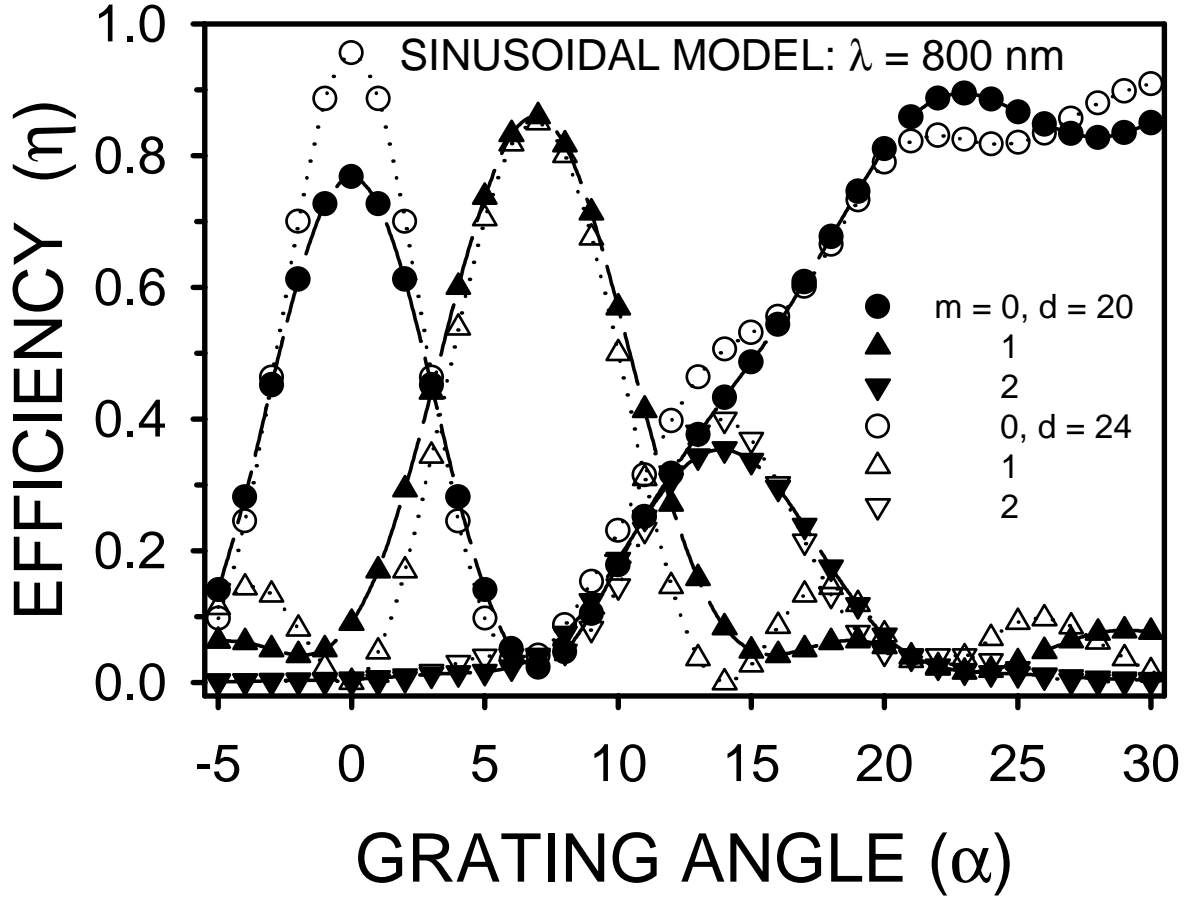


Fig. 6.— Sinusoidal RCWA predicted efficiency in unpolarized light for the  $300 \text{ l mm}^{-1}$  VPH grating (HG-T-1064-9) at 800 nm as a function of diffraction order ( $m$ ) and grating angle ( $\alpha$ ). Two grating thicknesses were modeled,  $d = 20$  and  $d = 24 \mu\text{m}$ . Neither case gives sufficient efficiency in the second order of diffraction.

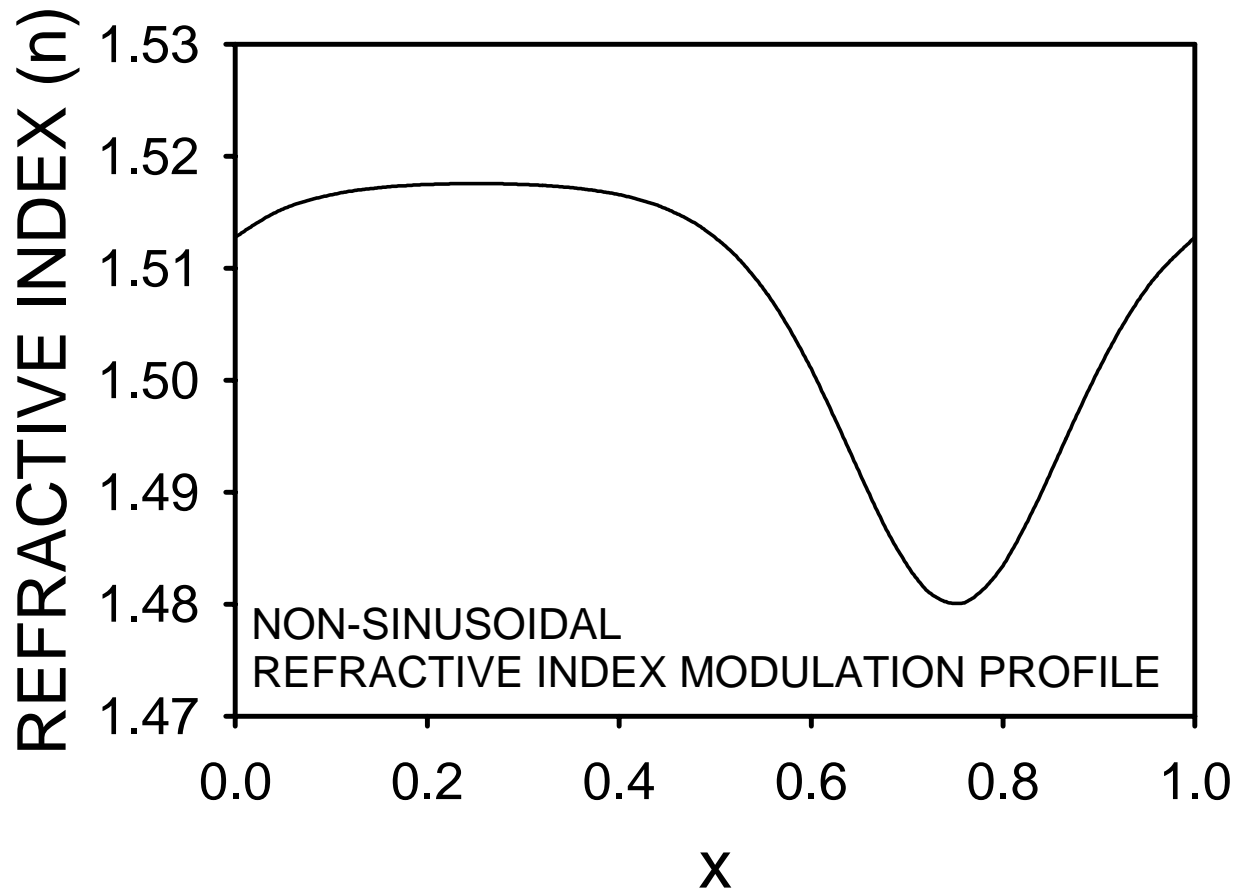


Fig. 7.— Non-sinusoidal index modulation profile used to better match the  $300 \text{ l mm}^{-1}$  VPH grating (HG-T-1064-9) efficiency with RCWA analysis.

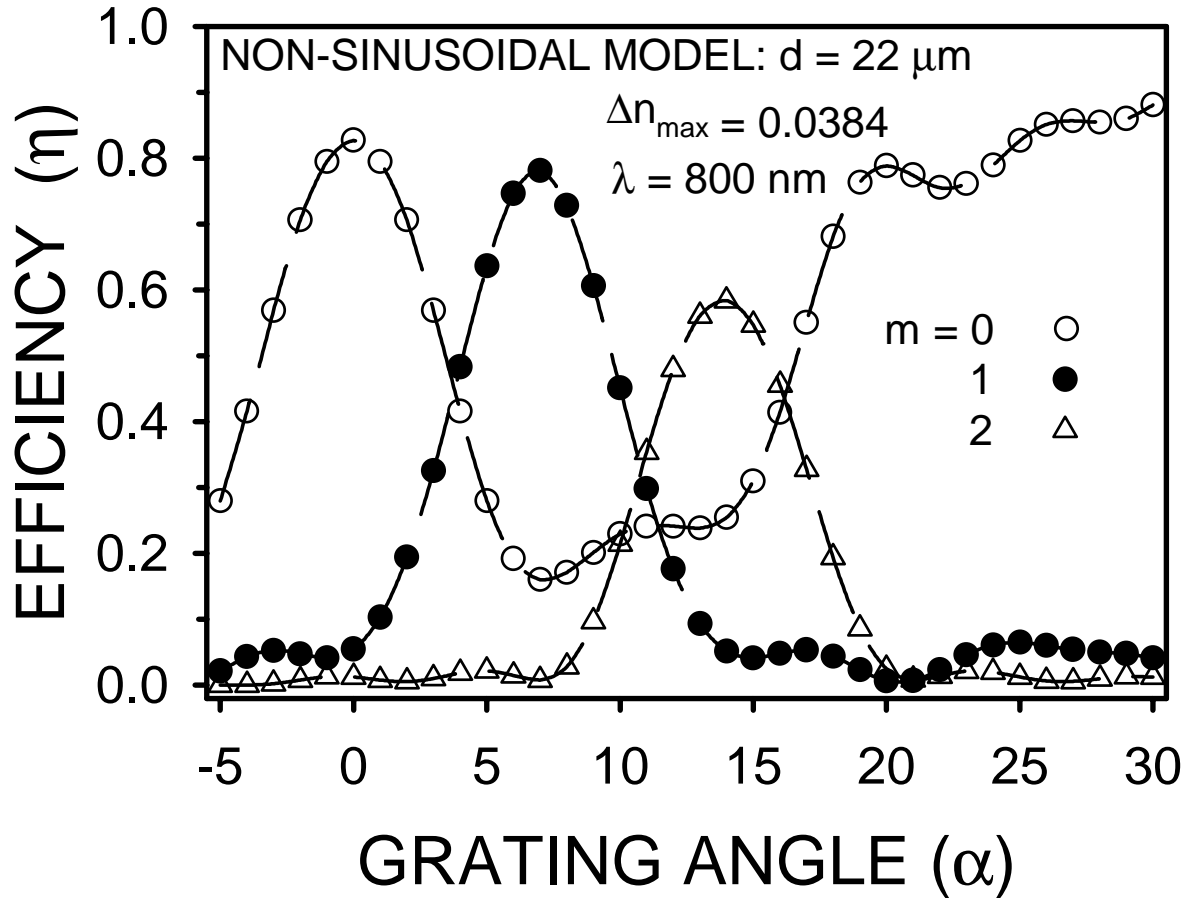


Fig. 8.— Non-sinusoidal RCWA predicted efficiency in unpolarized light for the  $300 \text{ l mm}^{-1}$  VPH grating (HG-T-1064-9) at  $800 \text{ nm}$  as a function of diffraction order ( $m$ ) and grating angle ( $\alpha$ ). This model provides a much better match to the real grating than do the purely sinusoidal models.

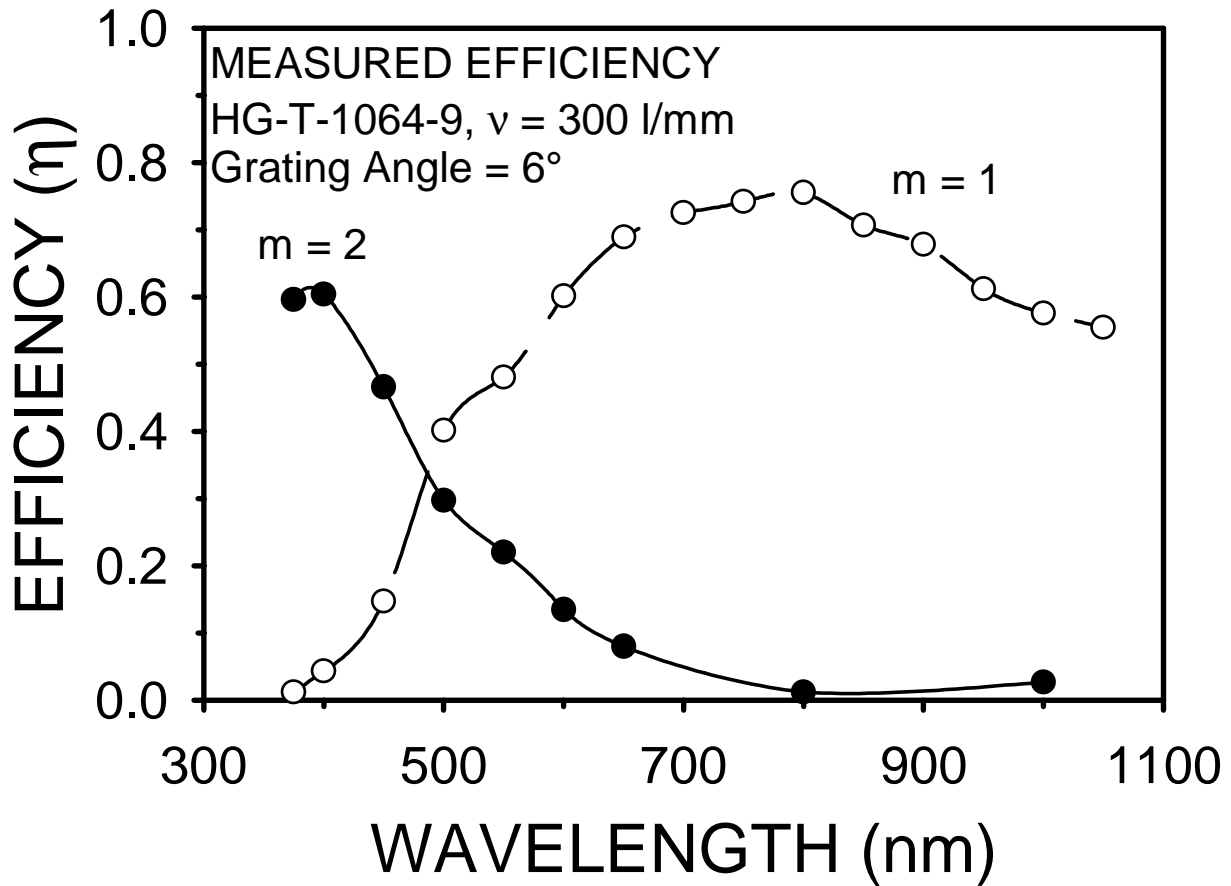


Fig. 9.— The “blaze” profile in unpolarized light for the  $300 \text{ l mm}^{-1}$  VPH grating (HG-T-1064-9) when tuned to a grating angle of  $6^\circ$ . These data include the losses due to the substrate material and surface reflection.

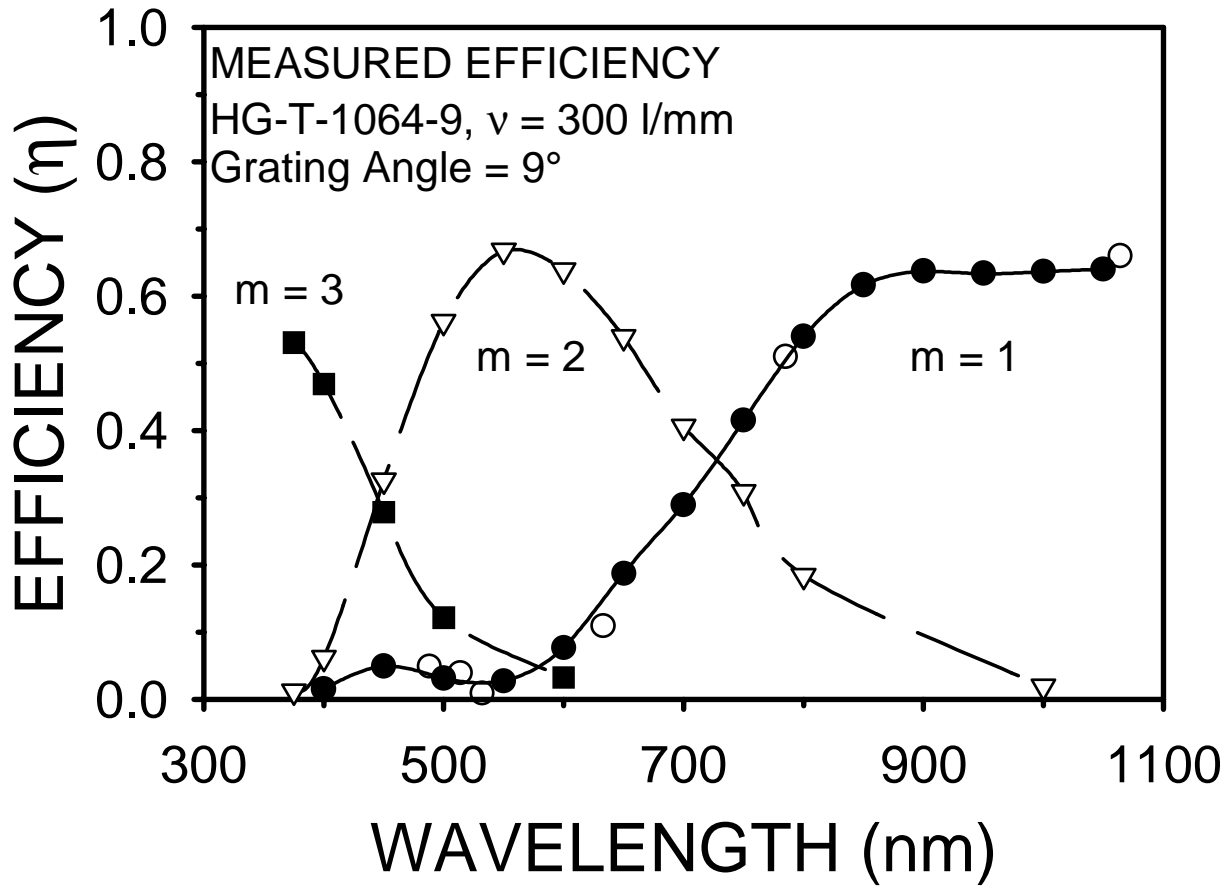


Fig. 10.— The “blaze” profile in unpolarized light for the  $300 \text{ l mm}^{-1}$  VPH grating (HG-T-1064-9) when tuned to a grating angle of  $9^\circ$ . The open circles are measurements made at KOSI for first order diffraction at a variety of laser wavelengths. These data include the losses due to the substrate material and surface reflection.

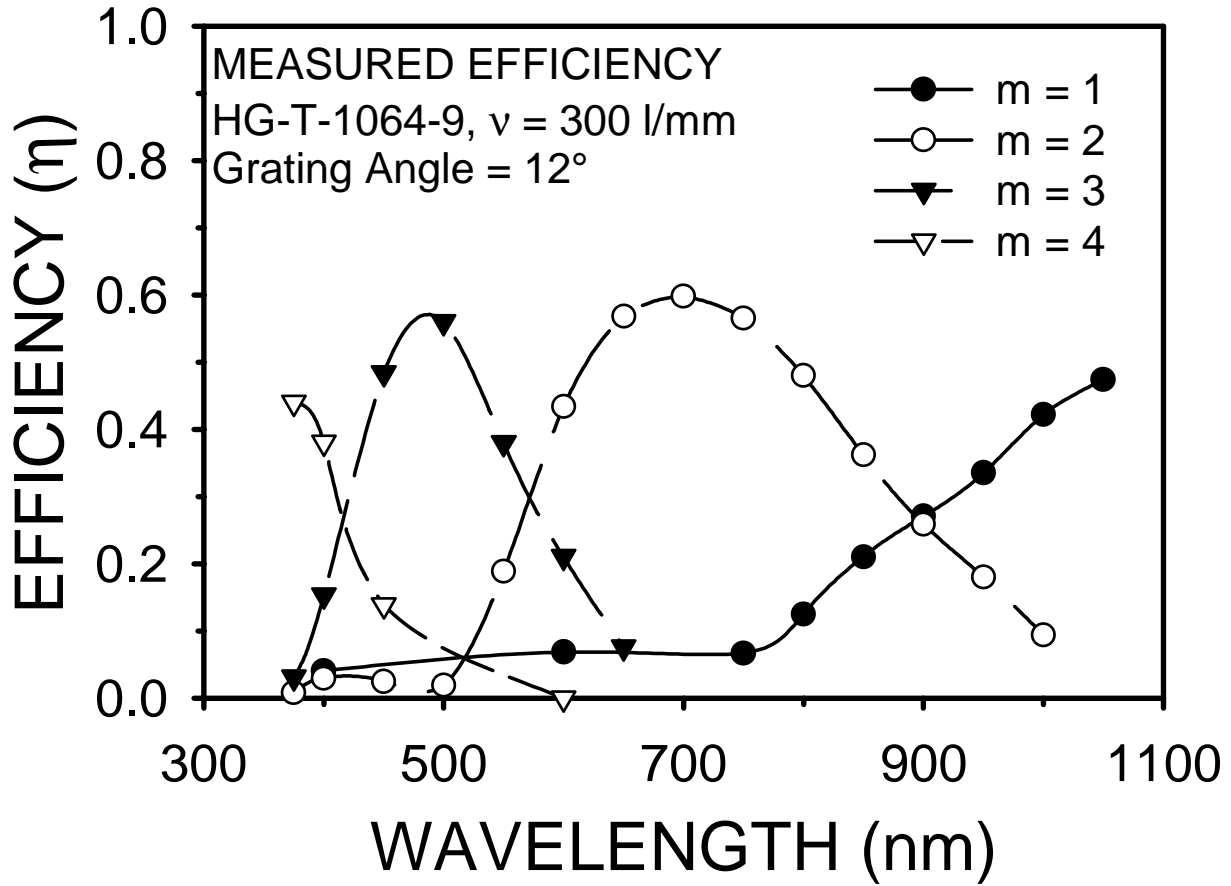


Fig. 11.— The “blaze” profile in unpolarized light for the  $300 \text{ l mm}^{-1}$  VPH grating (HG-T-1064-9) when tuned to a grating angle of  $12^\circ$ . Four orders of diffraction cover the optical spectral region. These data include the losses due to the substrate material and surface reflection.

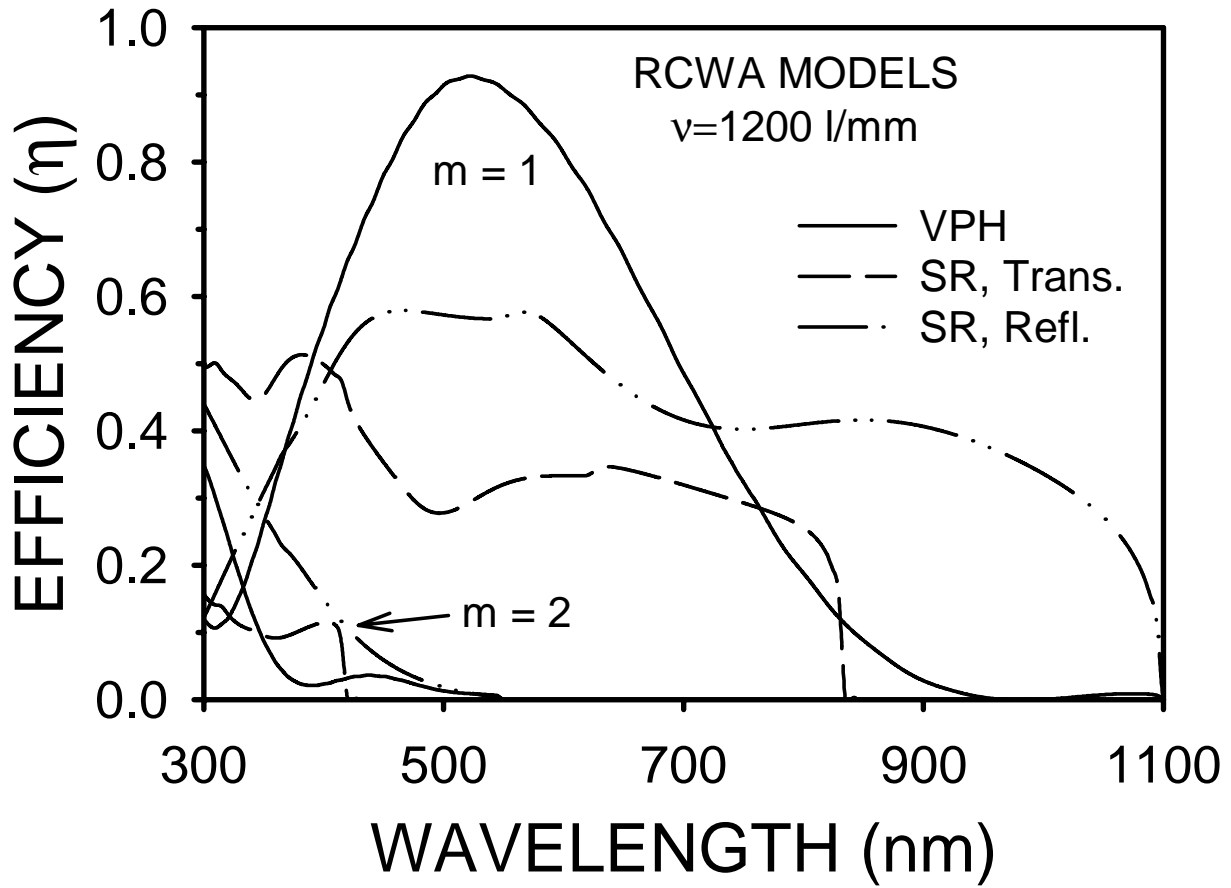


Fig. 12.— RCWA predicted efficiency for the  $1200 \text{ l mm}^{-1}$  VPH grating (HG-T-532-19) and comparable SR reflection and transmission gratings. A purely sinusoidal index modulation is assumed for the VPH grating.

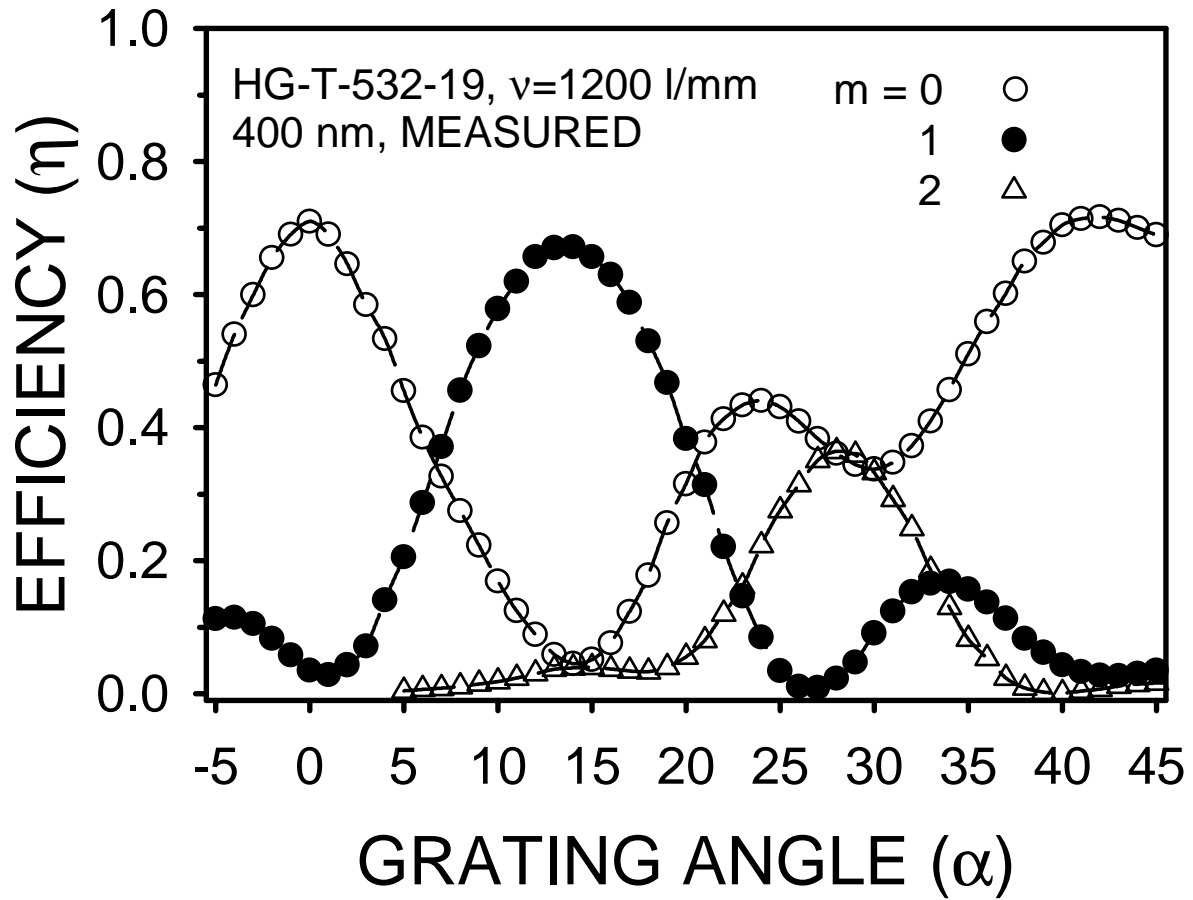


Fig. 13.— Measured absolute efficiency, inclusive of substrate material and surface reflection losses, in unpolarized light for the  $1200 \text{ l mm}^{-1}$  VPH grating (HG-T-532-19) at 400 nm as a function of diffraction order ( $m$ ) and grating angle ( $\alpha$ ).

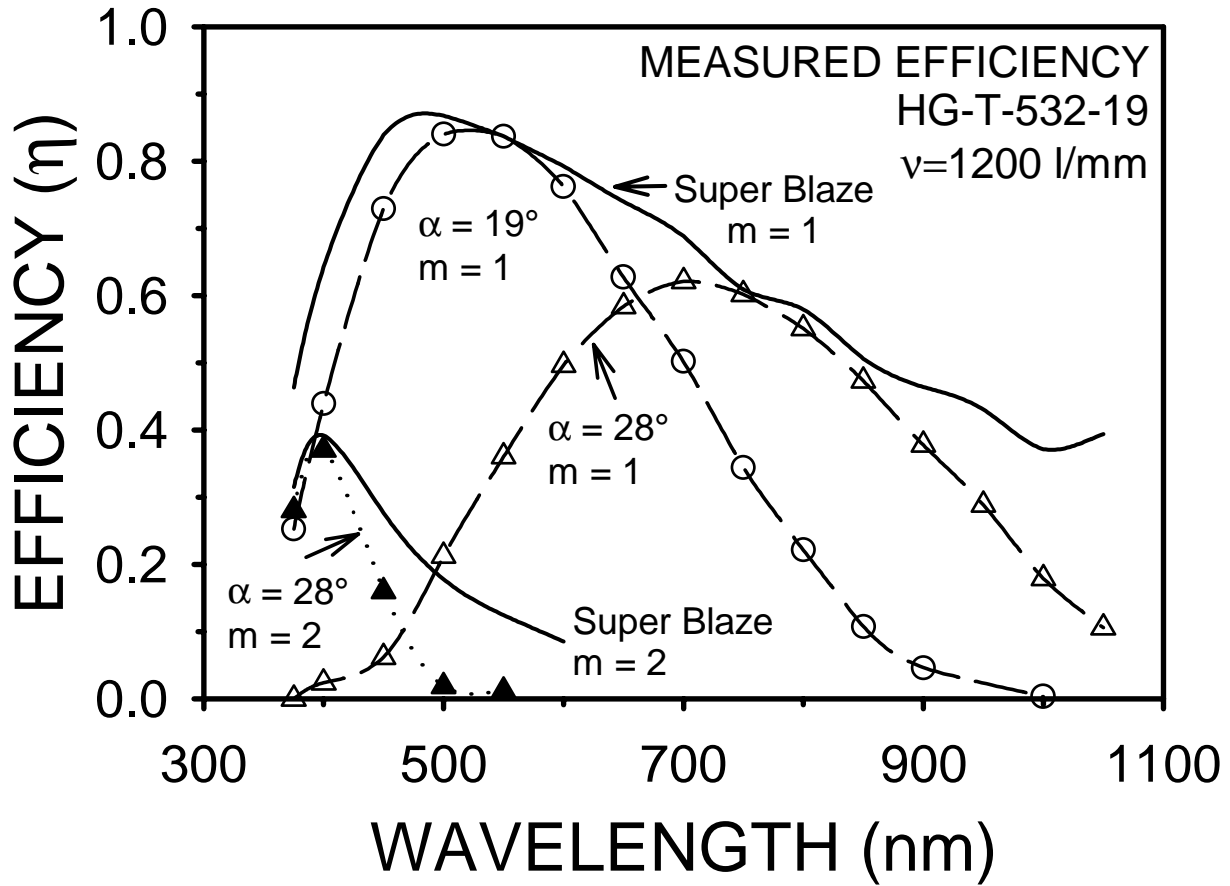


Fig. 14.— The “blaze” profile in unpolarized light, inclusive of substrate material and surface reflection losses, for the  $1200 \text{ l mm}^{-1}$  VPH grating (HG-T-532-19) when tuned to the design Bragg angle of  $19^\circ$ . The “superblaze” (see text) is also shown in the plot. Note that peak efficiency reaches nearly 87% when the grating is tuned to operate at a Bragg wavelength of 500 nm.

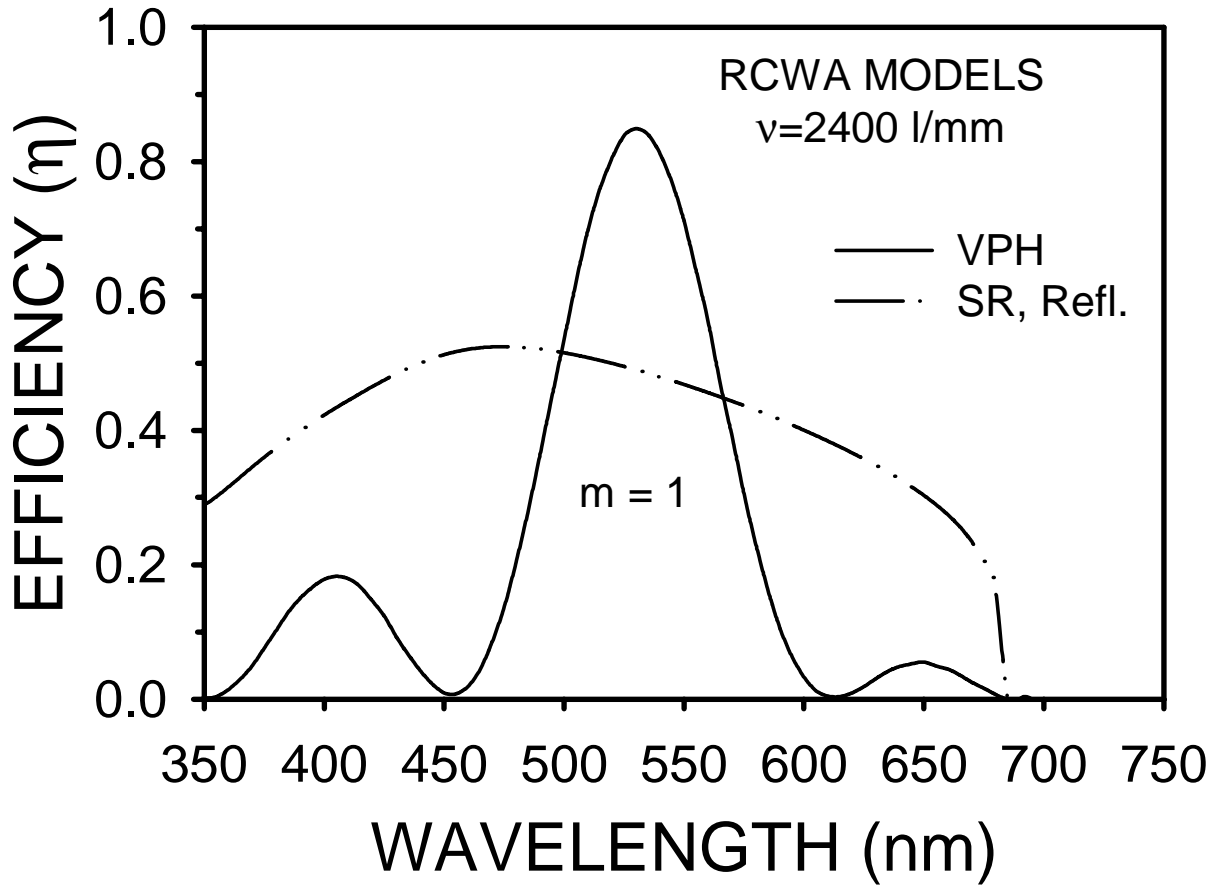


Fig. 15.— RCWA predicted efficiency for the  $2400 \text{ l mm}^{-1}$  VPH grating (HG-T-532-40) and a comparable SR reflection grating. A transmission SR grating is essentially impossible due to the steepness of the grating groove facets required to properly blaze such a grating. A purely sinusoidal index modulation is assumed for the VPH grating.

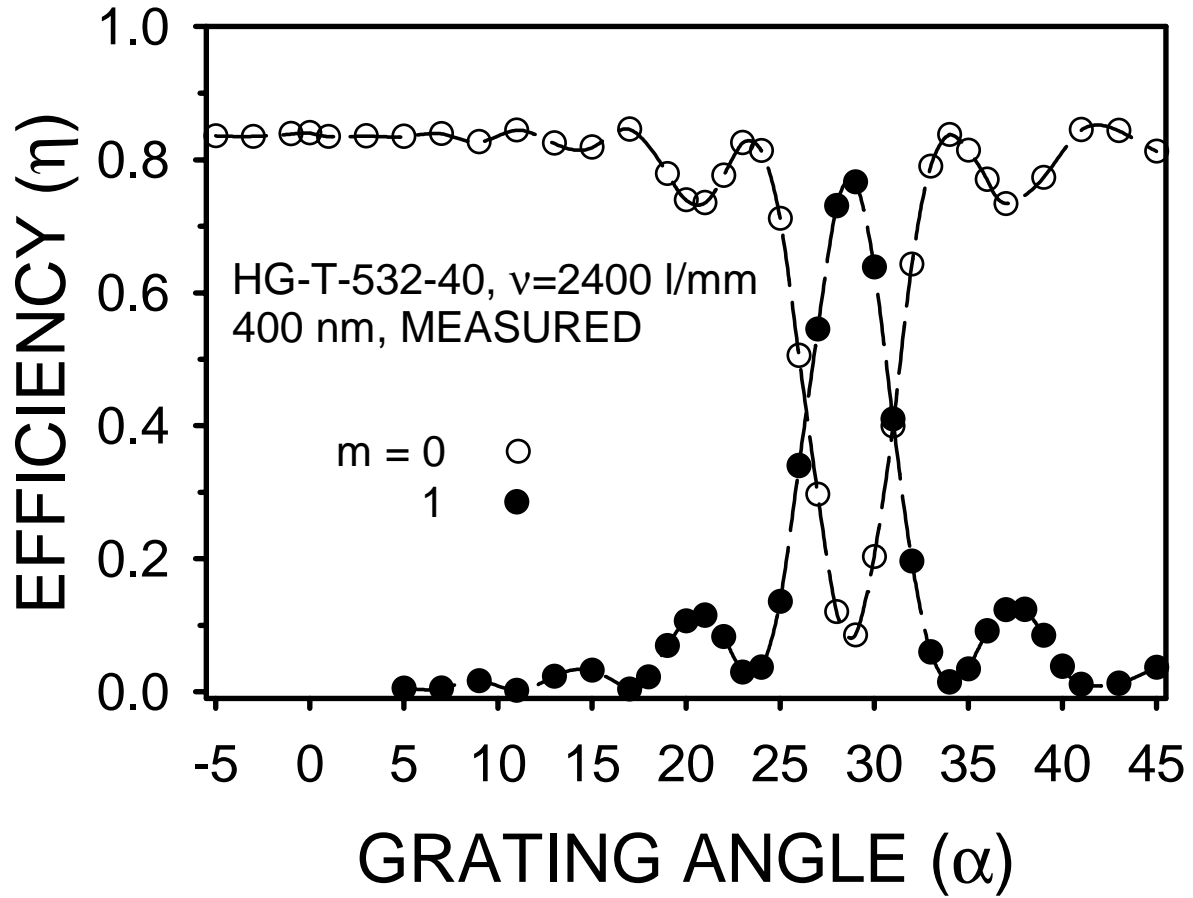


Fig. 16.— Measured absolute efficiency, inclusive of substrate material and surface reflection losses, in unpolarized light for the  $2400 \text{ l mm}^{-1}$  VPH grating (HG-T-532-40) at 400 nm as a function of diffraction order ( $m$ ) and grating angle ( $\alpha$ ).

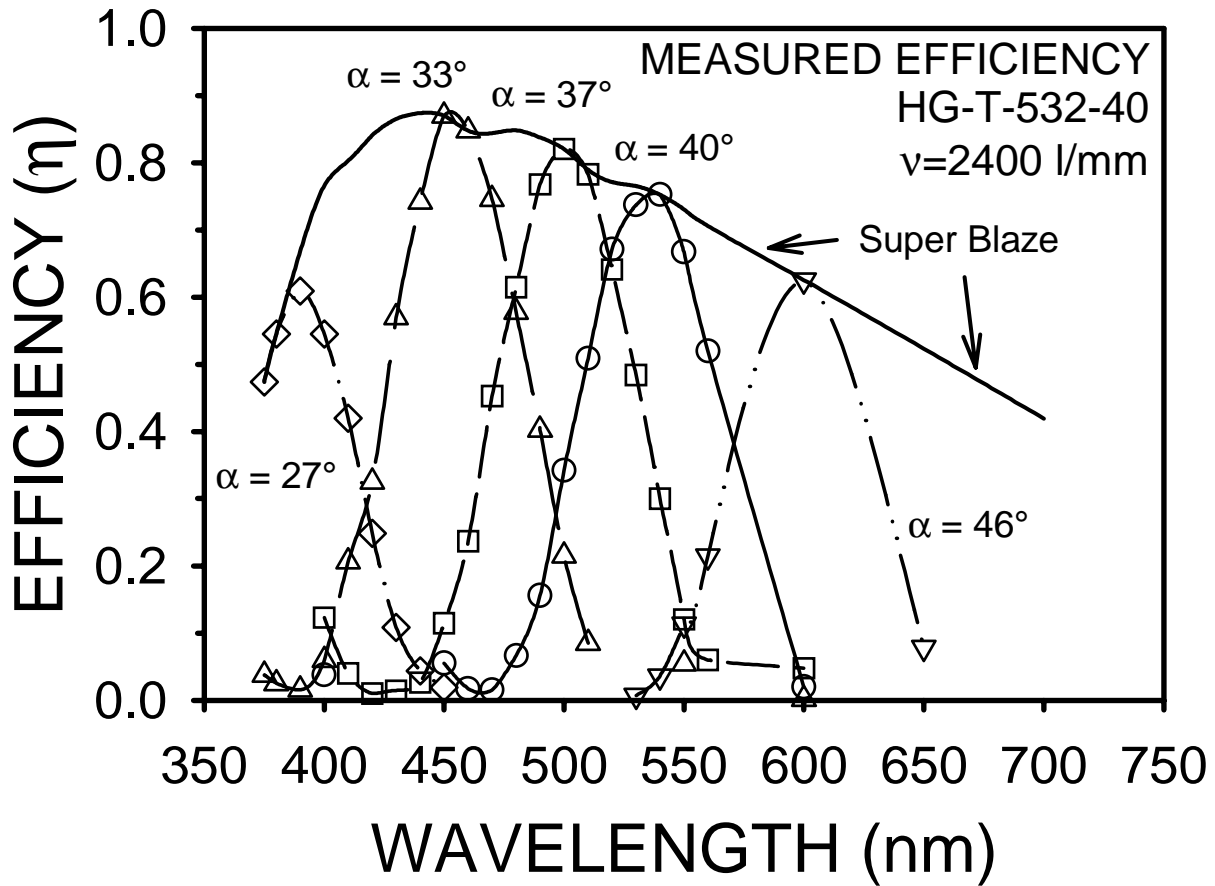


Fig. 17.— The “blaze” profile in unpolarized light, inclusive of substrate material and surface reflection losses, for the  $2400 \text{ l mm}^{-1}$  VPH grating (HG-T-532-40) when tuned to the design Bragg angle of  $40^\circ$ . The “blaze” for other grating angles is also shown along with the “superblaze” (see text). Note that peak efficiency reaches nearly 88% when the grating is tuned to operate at a Bragg wavelength of 440 nm.